Will SiOx-pinholes for SiOx/poly-Si passivating contact enhance the passivation quality?

Yang, Guangtao; Gram, Remon; Procel, Paul; Han, Can; Yao, Zhirong; Singh, Manvika; Zhao, Yifeng; Mazzarella, Luana; Zeman, Miro; Isabella, Olindo

DOI
10.1016/j.solmat.2023.112200

Publication date
2023

Document Version
Final published version

Published in
Solar Energy Materials and Solar Cells

Solar Energy Materials & Solar Cells 252 (2023) 112200

Contents lists available at ScienceDirect

Solar Energy Materials and Solar Cells

journal homepage: www.elsevier.com/locate/solmat

Will SiO_x-pinholes for SiO_x/poly-Si passivating contact enhance the passivation quality?

Guangtao Yang, Remon Gram, Paul Procel, Can Han, Zhirong Yao, Manvika Singh, Yifeng Zhao, Luana Mazzarella, Miro Zeman, Olindo Isabella *

Photovoltaic Materials and Devices Group, Delft University of Technology, Delft, the Netherlands

ARTICLE INFO

Keywords:
Poly-Si passivating Contacts
Pinhole density
Thermal diffusion budget
Enhanced passivation

ABSTRACT

Passivating contacts based on poly-Si have enabled record-high c-Si solar cell efficiencies due to their excellent surface passivation quality and carrier selectivity. The eventual existence of pinholes within the ultra-thin SiO_x layer is one of the key factors for carrier collection, beside the tunneling mechanism. However, pinholes are usually believed to have negative impact on the passivation quality of poly-Si passivating contacts. This work studied the influence of the pinhole density on the passivation quality of ion-implanted poly-Si passivating contacts by decoupling the pinhole generation from the dopants diffusion process by means of two annealing steps: (1) a *pre*-annealing step at high temperature after the intrinsic poly-Si deposition to visualize the formation of pinholes and (2) a *post*-annealing step for dopants activation/diffusion after ion-implantation. The pinhole density is quantified in the range of 1×10^6 to 3×10^8 cm^2 by the TMAH selective etching approach. The passivation quality is discussed with respect to the pinhole density and the post-annealing thermal budget (TB) for dopants diffusion. The study shows that a moderate pinhole density does not induce doping profile variations that can be detectable by the coarse spatial resolution of ECV measurements. It is surprising that the existence of pinholes in a moderate density within our thickness fixed SiO_x layer can effectively enhance the passivation qualities for both n^+ and p^+ poly-Si passivating contacts. We speculate the reason is due to the enhanced field-effect passivation at the pinhole surrounding. In fact, the variation of the passivation quality depends on the balance between a strengthened field-effect passivation and an excessive local Auger recombination, being both effects induced by the higher and deeper level of dopants diffused into the c-Si surface through the pinholes.

1. Introduction

Poly-Si carrier-selective passivating contacts for c-Si solar cells provide outstanding passivation quality and carrier selectivity as demonstrated in many high-efficiency solar cells architectures [1–12]. Their unique structure consists of two layers. An ultra-thin SiO_x layer chemically passivates the c-Si surface and builds up a potential barrier for the carriers' transport through it [13]. Then, a heavily doped poly-Si layer sits on top of the ultra-thin SiO_x layer. Owing to an optimized doping level, higher within the poly-Si layer and at the c-Si surface than in the c-Si bulk, an electrical field is built up at the c-Si interface, enabling field effect passivation and carrier selectivity [14,15]. The optimization of the doping tail inside the c-Si surface induces an efficient separation of carriers inside the c-Si bulk before they reach the c-Si surface where the defect density, D_{it}, is high. In practice, the doping tail is affected by the thermal diffusion budget (TB) [16] and the properties of the ultra-thin SiO_x layer [17]. However, when annealed at high temperature, the ultra-thin SiO_x layer can be locally broken to form pinholes, which will affect the doping tail and the D_{it} at the c-Si surface [13] as well as gettering efficacy against metal impurities [18]. Consequently, the formation of pinholes will influence the passivation quality of the poly-Si passivating contacts. In poly-Si processes one thermal process is conventionally used to activate/diffuse the dopants and to form pinholes in SiO_x, if any. This makes it difficult to study the effect of the SiO_x pinhole formation on the passivation quality. To investigate this topic, one needs to decouple these steps.

The most logical way for this decoupling is to use a two-step annealing processes. One annealing step is for inducing the formation of SiO_x pinholes; the second annealing step is used for dopant activation and diffusion. This approach was previously used by Gan et al. [19] to prepare poly-Si passivating contact and by Römer et al. [20] to study the contact resistivity of passivating contact stacks. In this contribution, we

* Corresponding author. Photovoltaic and Devices Group, Delft University of Technology, Mekelweg 4, 2628 CD, Delft, the Netherlands.
E-mail address: o.isabella@tudelft.nl (O. Isabella).

https://doi.org/10.1016/j.solmat.2023.112200
Received 8 September 2022; Received in revised form 3 January 2023; Accepted 10 January 2023
Available online 17 January 2023

effectively decoupled the process of forming pinholes from dopants diffusion by means of a two-step annealing process during the fabrication of our ion-implanted poly-Si passivating contacts. A *pre*-annealing step before ion-implantation is used to form the pinholes in the SiO_x layer. A second *post*-annealing step with different TB is used to activate the ion-implanted doping species and enable their diffusion. With a selective etching process based on TMAH [13,18], we monitored the density of the formed pinholes in the pre-annealing step. This enabled us to evaluate the influence of the presence of pinholes and the TB of dopants on the passivation quality of poly-Si passivating contacts.

2. Experimental and modelling

The poly-Si passivating contacts used in the work consist of thermally grown SiO_x layer (t-SiO_x) and an ion-implanted poly-Si layer grown with low pressure vapor deposition (LPCVD). The wafers used in this work are polished n-type float zone wafers with a resistivity of 1–5 Ω cm and thickness of 280 ± 20 μm. The t-SiO_x is fabricated with a Tempress furnace at a temperature of 675 °C in an oxygen containing atmosphere. The thickness of the t-SiO_x is 1.4 ± 0.1 nm, which is characterized on an <111> oriented, polished c-Si wafer by Ellipsometry Spectroscopy from J. A. Woollam. <111> oriented wafer is selected since the following passivation test samples are textured ones with <111> facets. The LPCVD poly-Si layer is deposited at 580 °C, with an as-deposited thickness of 100 ± 5 nm. The thickness of the poly-Si layers on flat wafers was calculated by knowing the deposition rate, which was obtained by measuring with ellipsometry spectroscopy the thickness of poly-Si deposited on flat wafer. While the deposition rate of poly-Si on textured surface is obtained by measuring the thickness of poly-Si layers on the pyramidal facets with SEM technique. The doping of the poly-Si layer is achieved with ion-implantation of phosphorus (P) or boron (B) for n^+ or p^+ type poly-Si, respectively. The ion-implantation parameters are energy = 20 keV (5 keV), dose = 6×10^{15} cm^{-2} (5×10^{15} cm^{-2}) for P (for B). To evaluate the pinhole density and its influence on the passivation quality of the poly-Si passivating contacts, we prepared two sets of samples: one for pinhole density characterization and one for passivation quality evaluation. As shown in Fig. 1(a) and (b), both sets of samples followed the same processes for the fabrication of t-SiO_x layer and poly-Si layer. The pinhole characterization samples are prepared on <100> double side flat wafers.

Following the deposition of LPCVD, intrinsic (i) poly-Si layers undergo the high-temperature (between 1000 °C and 1075 °C) pre-annealing step with the annealing time of 1 min at the peak temperature to form the pinholes in the t-SiO_x layer. The annealing process is conducted with a Tempress furnace, which enables a ramp-up and ramp-down rate of 10 °C/min. The temperature is monitored during all the annealing processes. A 5% TMAH based high selective etching step at 70 °C is used to visualize the pinholes, as shown in Fig. 2(a). The etching time is set to be 180 s, with which, for three tested samples, the standard error is around 3%. For the passivation quality evaluation samples, textured n-FZ wafers are used. Before the ion-implantation of P or B species on both sides of the wafers, the samples with (i) poly-Si layers are pre-annealed with the same setting as the pinhole samples. After ion-implantation, a post-annealing step is used to activate and diffuse the dopants [6]. The hydrogenation of these passivation samples is done before evaluating the passivation quality. This is done by first depositing a PECVD SiN_x capping layer (in the role of H-source) and then performing forming gas annealing step at 400 °C for 30 min.

After TMAH etching, the pinhole samples prepared with different pre-annealing temperatures are characterized with an optical microscope. With photos area of 100 μm × 100 μm, the pinhole density is carried out as a function of the pre-annealing temperature. The averaged pinhole density values are obtained from three samples. The minority carriers lifetime and implied open-circuit voltage (iV_{OC}) of the samples were analyzed by means of a Sinton WCT-120 lifetime tester applying the generalized measurement mode [21].

The main objective of this work is to assess the relationship between pinholes density, doping distribution, electric field at the SiO_x/c-Si interface and passivation quality. Next to visualizing and generally counting the pinholes density as well as reporting the ECV profiles alongside the lifetime measurement, we also performed a simulation campaign. By means of our TCAD Sentaurus modelling framework [15], we can explain the electric field difference at the SiO_x/c-Si interface for different samples characterized by different pre- and post-annealing conditions. Accordingly, we consider a simulated structure which consists of poly-Si layer on top of a SiO_x film over a c-Si n-type wafer. We use measured thickness and ECV doping profiles as input parameters to calculate the electric field given a charge distribution by solving Poisson's equation. We note that the electric field depends on the differential of the charge distribution (doping profile) in the space domain rather than charge magnitude. For instance, one can expect that the electric field is relatively low inside highly doped poly-Si film where the doping profile is almost constant in such a region. Similarly, relatively high electric field values are expected where the doping profile exhibits steeper variations near the SiO_x/c-Si interface.

3. Results and discussions

3.1. Pinhole density

Optical images of the pinhole samples are shown in Fig. 2(a1-a4). After 1 min annealing at 1000 °C, we observed much fewer pinholes

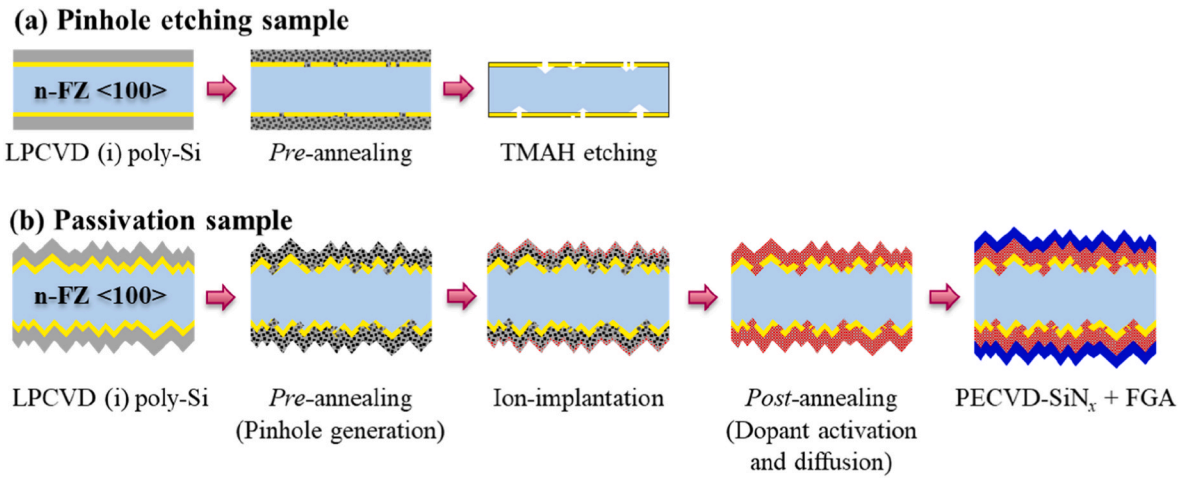

Fig. 1. Schematic sketches of the processes to manufacture (a) pinhole density characterization samples and (b) passivation quality evaluation samples.

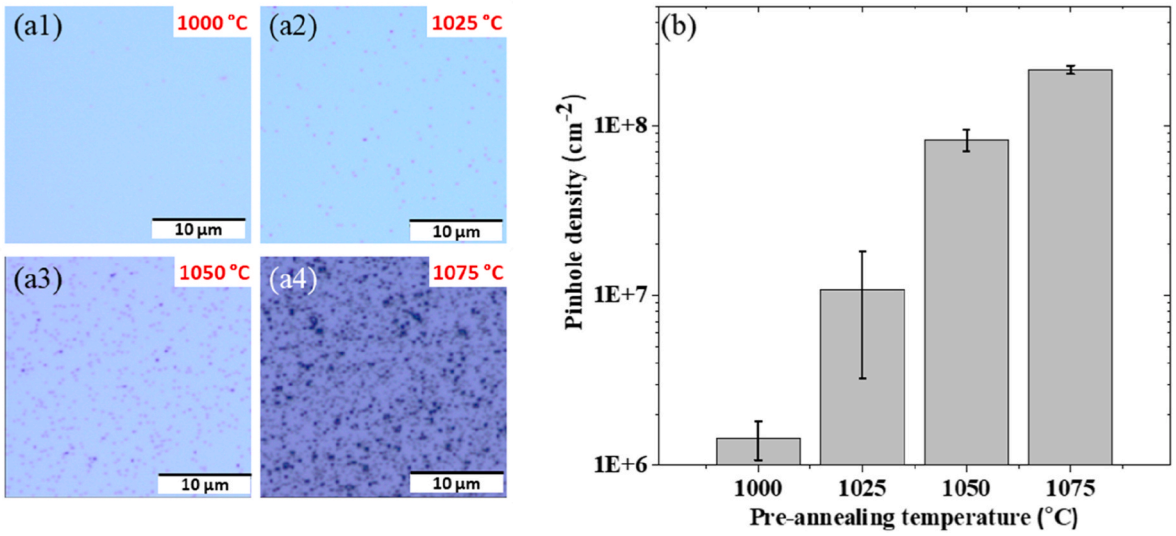

Fig. 2. Optical microscope top view images of etched-back poly-Si samples prepared with pre-annealing for 1 min at temperature of (a1) 1000 °C, (a2) 1025 °C, (a3) 1050 °C, and (a4) 1075 °C, according to which the calculated pinhole density as a function of the pre-annealing temperature is plotted in (b). The averaged pinhole density values are obtained from 3 samples manufactured per each pre-annealing temperature.

than in other cases annealed at higher temperatures (1025 °C, 1050 °C, and 1075 °C). Accordingly, the calculated pinhole density values as a function of the pre-annealing temperature are plotted in Fig. 2(b). From that we can see the pinhole density values increase with the pre-annealing temperature, dramatically, with a fixed annealing time. This trend and the related pinhole density values, between 1×10^{6} and 2×10^{8} cm^{-2}, are consistent with literature [22–24]. For the post-annealing, when the temperature is lower than 1000 °C the pinhole density variation due to the post-annealing will be too low to be recognized. Therefore, the pinholes eventually generated in that temperature regime will not have a significant impact on the doping profile. For post-annealing temperatures above 1000 °C, the pinholes generated will negatively affect the passivation quality as shown in following sections.

3.2. Thermal diffusion budget

During the post-annealing step after the ion-implantation, the dopants are activated and diffused within the poly-Si material and, through the t-SiO_x, the c-Si material. The diffusion within the c-Si bulk is crucial, as it affects the tail of the doping profile, which is one of the key factors that dominate the electrical field passivation quality, as well as the Auger recombination. The parameters that affect the doping profile are the annealing temperature and time as well as the properties of the t-SiO_x, including its thickness, density, pinhole density, etc. The thermal diffusion budget (TB) is widely used in the semiconductor industry to illustrate the diffusion of dopant within a semiconductor material with respect to the annealing settings [16]. Following the decoupling of the pinhole generation and the dopants diffusion steps, we introduced the concept of TB to the poly-Si based passivating contact process for a specific post ion-implantation annealing temperature (T_i) [16]:

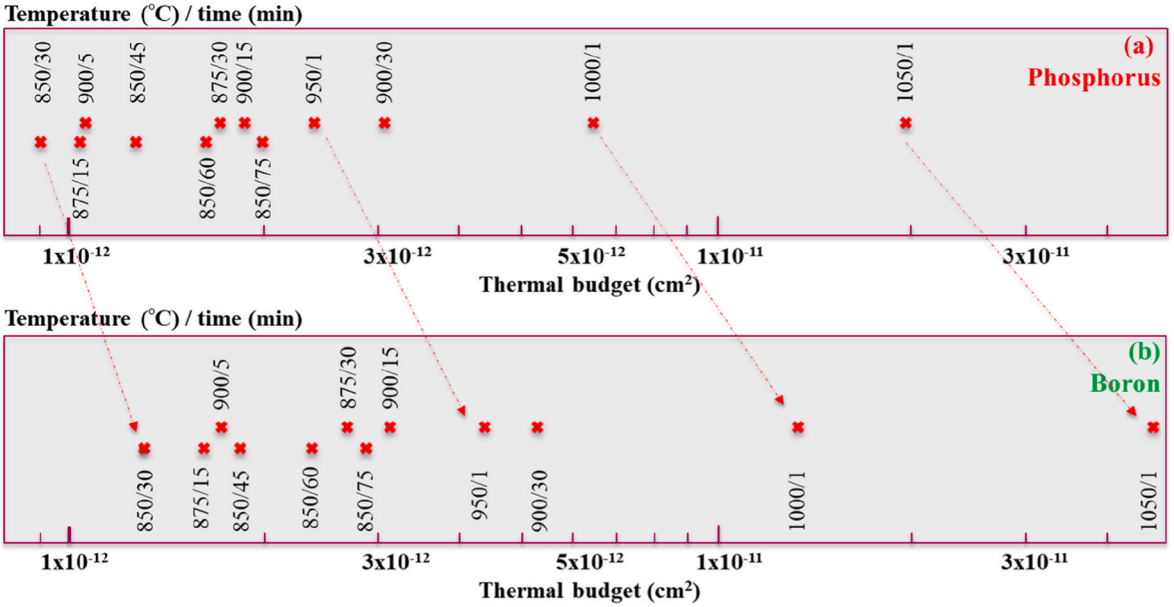

Fig. 3. The calculated diffusion thermal budget values according to the post-annealing settings, temperature (°C) and time (min), for (a) P and (b) B in c-Si material.

$$TB_i = D_0 e^{-\frac{E_a}{k_B T_i}} \cdot t \quad (1.1)$$

where t is the post ion-implantation annealing time, D_0 is the diffusion constant, and E_a is the dopant activation energy. Owning to the difference in value of D_0 (8×10^{-4} cm^2/s for P and 6×10^{-2} cm^2/s for B [25]) and E_a (2.74 eV for P and 3.12 eV for B [25]), the TB for B is around 2 times higher than that for P when the same post-annealing settings are used as shown in the double x-axis of Fig. 3(a) and (b), as a result different passivation quality is expected. This indicates different diffusion dynamics between P and B in c-Si material. The physical unit of TB is cm^2, which is interpreted as the squared diffusion length of the dopants [16]. On the other hand, the D_0 of P and B within thermal SiO_2 layer is in the level of more than 10^{16} cm^2/s [26], which is much higher than that within Si materials; therefore, we did not consider the diffusion of dopants within the thermal SiO_x layers as a limiting factor.

3.3. Passivation quality and thermal budget

We prepared symmetric, textured samples endowed n^+ poly-Si passivating contact layers (see Fig. 1) with the same pre-annealing and post-annealing settings as those for the pinhole density characterization samples and for the TB values calculation. After hydrogenation with SiN_x capping layer and FGA annealing, the passivation quality of the samples is plotted in the *passivation quality diagram* (see Fig. 4). There, we map the pinhole density on the pre-annealing temperature (for 1 min annealing) as well as the TB on the post-annealing temperature/time settings versus the iV_{OC} of the passivation quality evaluation samples. We generally observe that (i) samples experiencing too large TB show much lower passivation quality than those experiencing moderate TB values; (ii) samples with pinholes show higher passivation quality than those samples without pre-formed pinholes in the t-SiO_x layer; (iii) there is a process window where the pinhole density and TB are at the moderate region, which delivers the optimal passivation quality.

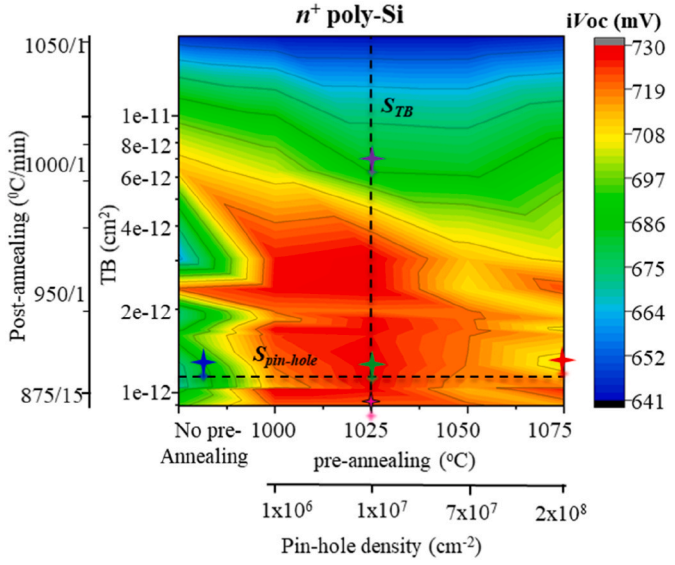

Fig. 4. The passivation quality diagram maps the pinhole density on the pre-annealing temperature (for 1 min annealing) and the TB on the post-annealing temperature/time settings versus the iV_{OC} of the passivation quality evaluation samples. The pinhole density values were characterized from the flat wafers, while the calculated TB values for n^+ poly-Si samples were prepared on double side textured c-Si wafers. The reported iV_{OC} values were measured after the hydrogenation step without removing the SiN_x capping layer. S_{TB} and $S_{pinhole}$ are two series of samples in which we varied TB for a fixed pinhole density or pinholes density for a fixed TB, respectively. The colored stars overlaid on the diagram indicate the samples used for studying ECV profiles in Figs. 5 and 7.

From such diagram we pick one series of samples prepared with the same pre-annealing settings but different post-annealing TB values (series S_{TB}). These three samples experienced the same pre-annealing at 1025 °C for 1 min. The pinhole density formed at this step is 1×10^7 cm^{-2} (see Fig. 2(b)). In this specific series, the sample with the highest TB is post-annealed at 1000 °C for 1 min. The maximal additional pinhole density due to such post-annealing is expected to be ~1.5×10^6 cm^{-2} (see Fig. 2(b)), which is only around one tenth of the value that was formed with the pre-annealing step. Therefore, we expect the similar pinhole density for all these three samples.

As expected, by increasing TB, the dopants diffusion into the c-Si bulk is more pronounced. This can be seen in Fig. 5(a) from their measured doping profile curves. Fig. 5(b) reports the corresponding calculated electric field profiles. Samples prepared with lower TB, that are post-annealed at 850 °C or 875 °C, show similar doping profile and doping tails within the c-Si bulk. In other words, with these low TB processes, the diffusion through the t-SiO_x and pinholes is limited due to the corresponding low dopant diffusion length. However, increasing the TB values by about 3 times, as in case of the sample post-annealed at 1000 °C, the doping tail within the c-Si surface becomes rather pronounced and deep. Such deep doping tail within the c-Si surface induces a lower passivation quality, as can be seen from the lifetime curves shown in Fig. 5(c) due to the increase of Auger recombination in highly doped profiles.

On the other hand, the sample with post-annealing at 875 °C shows higher passivation, even though its ECV doping profile curve is nearly identical with the one post-annealed at 850 °C. Such an effect is ascribed to the improved field effect passivation for this sample as Fig. 5(b) depicts. As the pinhole density is similar in these samples, we believe that the slightly higher TB of the post-annealing at 875 °C provides better dopants diffusion through the pinholes, as illustrated in the literature [27,28]. This is presented in Fig. 6(a). When post-annealing with the lowest TB condition, there is just a minor excess of dopants diffusion through the pinhole to the c-Si surface (see Fig. 6(a1)). When increasing the TB condition to 875 °C post-annealing, the dopant diffusion through the pinholes increases (see Fig. 6(a2)). However, such excess of dopants within the c-Si surface is not enough to be recognized by the ECV measurement, which characterizes the averaged doping level of an area with a diameter in the scale of a few mm. That is why we observed two identical doping profiles for the samples post-annealed at 850 °C and 875 °C despite exhibiting different passivation levels. This effect is attributed to the stronger field effect passivation for the higher TB sample, induced by the excess dopants at the pinhole areas of the c-Si surface. When increasing the post-annealing temperature to 1000 °C, even more dopants diffuse through the t-SiO_x layer and, of course, through the pinholes. This is now so pronounced that the ECV doping profile clearly exhibits a deep doping tail within the c-Si surface. In our illustration in Fig. 6(a3), these dopants at the c-Si surface further enhance the electrical field to maximize the field effect passivation. However, they also induce a much higher Auger recombination, which cannot be compensated by the enhanced field effect passivation. Consequently, the observed passivation quality is lower compared to the two samples with lower TB.

3.4. Passivation quality and pinhole density

To further discuss the relation between the pinhole density and the passivation quality of the poly-Si passivating contact, we choose a series of samples characterized by medium TB (post-annealing at 875 °C for 30 min) with varying the pinhole density (see $S_{pinhole}$ series in Fig. 4). In this way we can discuss the influence of pinhole density on the passivation quality by simply adjusting the pinhole density with varying the pre-annealing temperature from no pre-annealing (pinhole density ≈ 0 cm^{-2}), to 1025 °C (pinhole density ≈ 1×10^7 cm^{-2}) and 1075 °C (pinhole density ≈ 2×10^8 cm^{-2}) pre-annealing temperature settings. As shown in Fig. 7(a), samples with no pinholes and with pinhole density 1×10^7

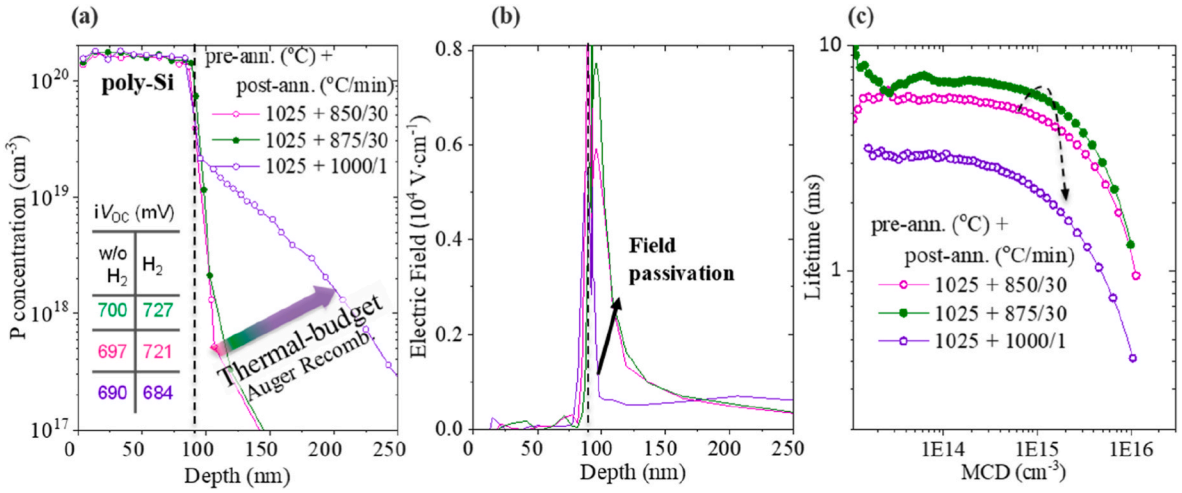

Fig. 5. The ECV doping profile (a) and the calculated electric field profile (b) of the post-annealing TB series (S_{TB}) samples. Corresponding iV_{OC} values extracted from lifetime curves measurements in (c) are inserted in (a).

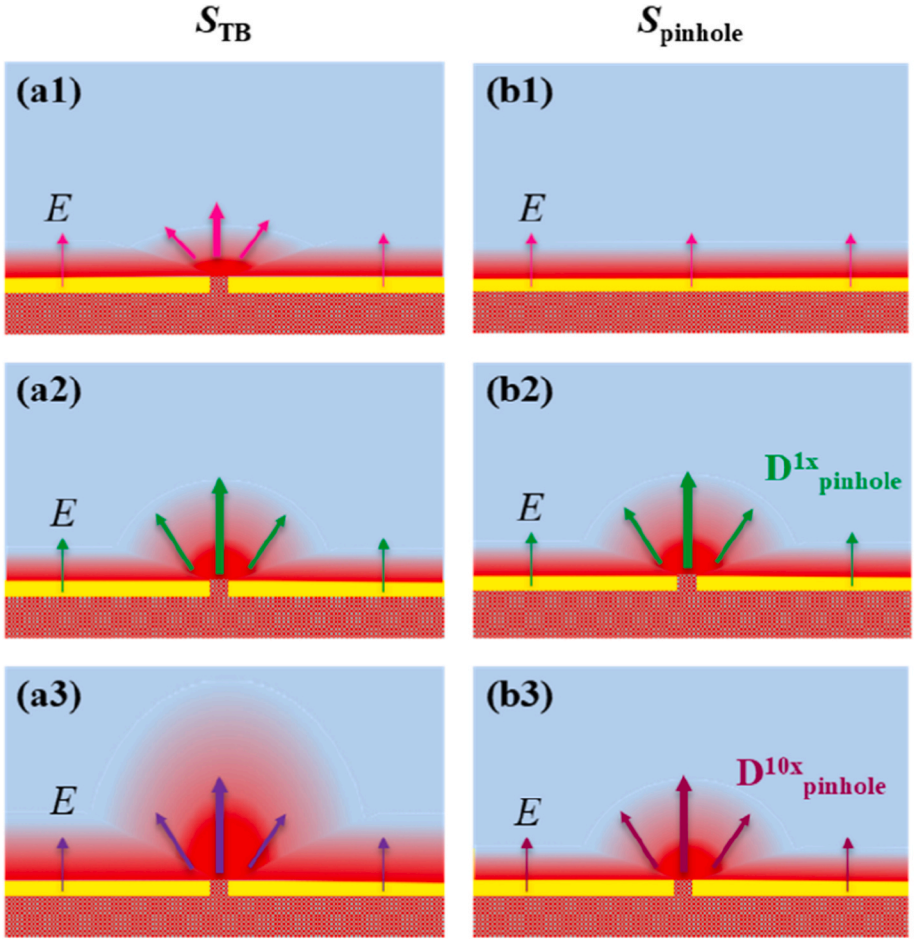

Fig. 6. Sketches for the electrical field, E, at the interfaces of poly-Si/t-SiO_x/c-Si for the thermal budget series (S_{TB}) (a1 = low TB, a2 = medium TB, a3 = high TB) and for the pinhole density series ($S_{pinhole}$) (b1 = no pinholes, b2 = low pinholes density, D^{1x}, b3 = high pinholes density, D^{10x}).

cm^{-2} exhibit similar ECV doping profiles. However, the calculated electrical field at c-Si interface is different as Fig. 7(b) illustrates. Therefore, the sample with low pinhole density shows much higher passivation quality than the one without pinholes, see Fig. 7(c). This can be argued similarly as in the previous section: for the sample with pinholes, the excess of dopants diffusion into the c-Si surface is not recorded by the ECV measurement technique, but it is crucial to enhance the field effect passivation (see Fig. 6(b1) and (b2) and Fig. 7(b)). On the other hand, for the sample with higher pinhole density (2×10^8 cm^{-2}, pre-annealed at 1075 °C), the volume of the excess dopants that diffuse through the pinholes within the c-Si bulk is pronounced and can be recorded by the ECV measurement technique, (see Fig. 7(a)). According

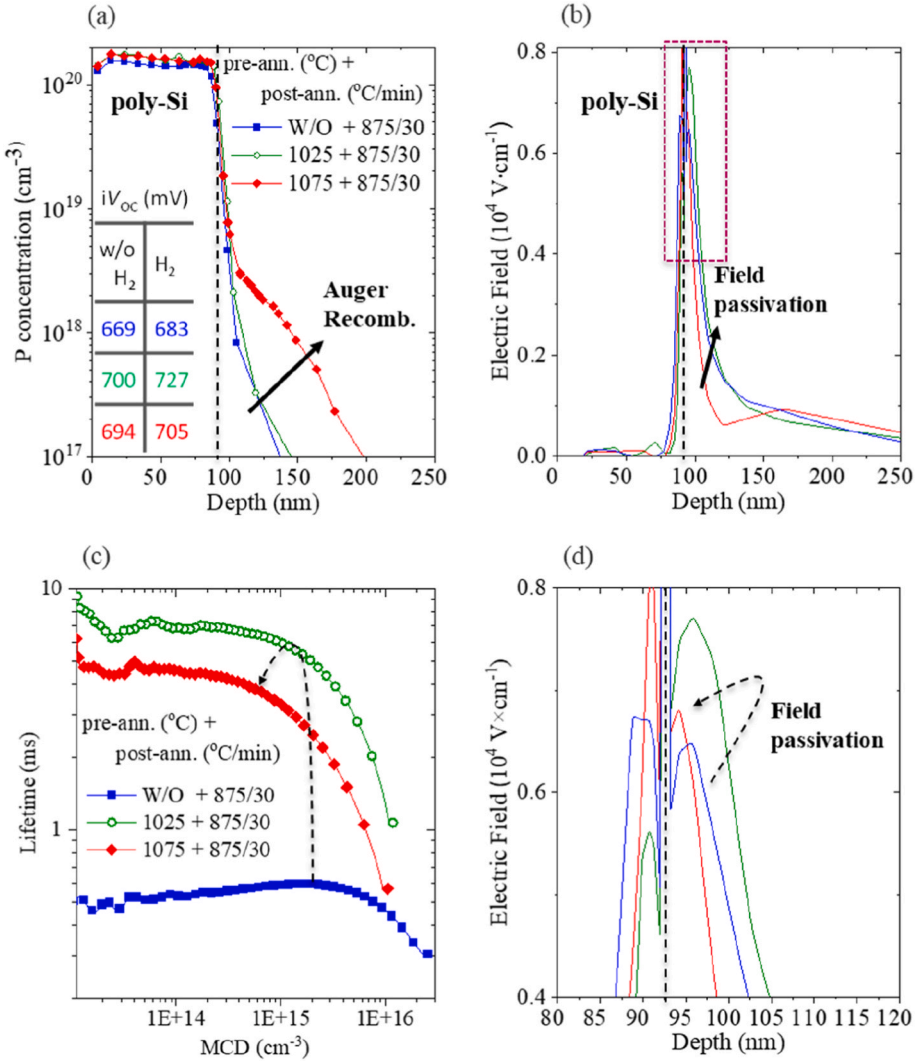

Fig. 7. The ECV doping profile (with iV_{OC} in the inset) (a) with calculated electric field profile (b) and (c) the lifetime curves for the pinhole density (pre-annealing) series ($S_{pinhole}$) samples. The curves in the dashed box in (b) are zoomed in (d).

to Fig. 6(b3) and Fig. 7(b), these excess dopants at the c-Si surface enhance the electrical field, which is beneficial for the field effect passivation, but also induce extra Auger recombination at the c-Si surface region of the bulk. Because the level and depth of these dopants are not so high as in case of the sample with the highest TB shown in Fig. 5 (a), the Auger recombination is limited. Therefore, compared to the sample without pinholes, the overall passivation of this sample with high pinhole density is still much higher. However, when moving to higher post-annealing TB settings, passivation quality of the samples with the same pre-annealing settings show a deceasing trend, as is shown in Fig. 4. Looking at Fig. 7(b), the sample without pre-annealing seems to yield electric field at the SiO_x/c-Si interface similar to that of the pre-annealed sample at 1075 °C, while its passivation is significantly lower. However, zooming-in the electric field curves around the SiO_x/c-Si interface as in Fig. 7(d) and looking at their intensities after said interface, we confirm the same lifetime trend as shown in Fig. 7(c).

Note that the results reported in this work, which are based on thermally grown SiO_x layer, may not apply to other types of ultra-thin SiO_x. For example, attempting a similar study on NAOS- SiO_x [6], the pre-annealing approach proved not conclusive as previously discussed in the literature [29].

3.5. Passivation quality of p^+ poly-Si

With the same pre- and post-annealing settings, we also prepared symmetric, textured samples endowed p^+ poly-Si passivating contact layers. The *passivation quality diagram* as function of pre- and post-annealing conditions is reported in Fig. 8(a). In general, the passivation quality of the p^+ poly-Si passivating contacts is lower than that of the n^+ poly-Si samples. We note that samples which experienced too high TB show much lower passivation quality than that of samples prepared at lower TB values. While samples with pinholes show slightly higher passivation quality than that of the samples prepared without intentionally pre-forming pinholes in the t-SiO_x layer. There is also an optimal passivation quality window, for which both the pinhole density and the TB have moderate values. This is also in-line with previous literature, that within an optimum pinhole density window, the pinhole density could have little impact on the doping profile, but may positively impact the passivation quality [28,30]. However, the sensitivity of the passivation quality on the pinhole density for p + poly-Si samples is much lower than in case of n + poly-Si samples. This is related to boron which readily diffuses through the SiOx into the silicon, leading to a lower surface passivation [30].

Following the same procedure as in Section 3.3 and Section 3.4, we picked up the two series of samples: the TB series and the pinhole density series (S_{TB} and $S_{pinhole}$ curves shown in Fig. 8(a), respectively). From the

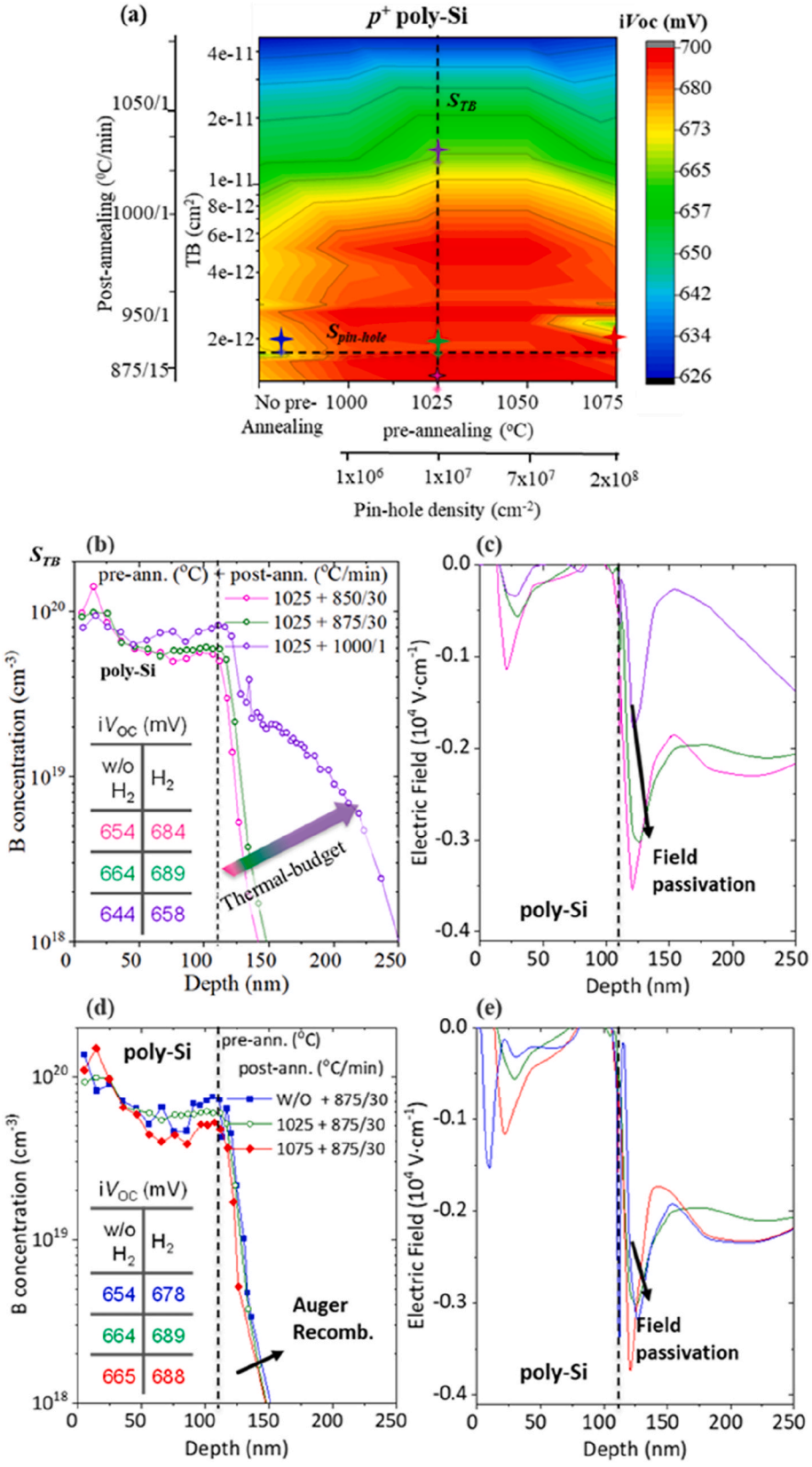

Fig. 8. (a) Passivation quality diagram maps the pinhole density on the pre-annealing temperature (for 1 min annealing) and the TB on the post-annealing temperature/time settings versus the iV_{OC} of the evaluation samples. The pinhole density values were characterized from the flat wafers, while the calculated TB values for $p+$ poly-Si samples were prepared on double side textured c-Si wafers. The reported iV_{OC} values were measured after the hydrogenation step without removing the SiN_x capping layer. S_{TB} and $S_{pinhole}$ are two series of samples in which we varied TB for a fixed pinhole density or pinholes density for a fixed TB, respectively. The colored stars overlaid on the diagram indicate the samples used for studying ECV profiles. The ECV doping profile (with iV_{OC} in the inset) and the calculated electric field profiles of the S_{TB} and $S_{pinhole}$ series samples are reported in (b and d) and (c and e), respectively.

ECV curves and the iV_{OC} values of the S_{TB} series samples, we can draw similar conclusions to those about the n^+ poly-Si samples. As reported in Fig. 8(b) and (c), the doping profile and the calculated electric field is sensitive to the post-annealing TB. For TB $> 5\times10^{-12}$ cm^2 the passivation quality (iV_{OC}) drops tremendously due to enhanced Auger recombination induced by the excess B diffusion into the c-Si surface. While for lower TB values similar ECV profiles yield similar and higher passivation quality due to the enhanced electric field as Fig. 8(c) shows.

As for the $S_{pinhole}$ series, the conclusion found for n^+ poly-Si is still valid: compared to the non-pinhole samples, the existence of pinholes helps to enhance the overall passivation (see Fig. 8(d)). In fact, despite the three samples exhibit similar ECV profiles, only the samples with intentionally pre-formed pinholes result in higher iV_{OC}. This is again attributed to the trade-off between Auger recombination and electric field passivation at the pinhole area due to the excess B diffusion.

4. Conclusion

In this work, we decouple the pinhole formation step from the dopants' diffusion step during the fabrication processes of poly-Si passivating contacts by adding an extra pre-annealing before the dopants' implantation in the intrinsic poly-Si layer. The pinholes formed with the pre-annealing are visualized by a TMAH selective etching. The images show that the pinhole density increases with higher pre-annealing temperature. By introducing the concept of post-annealing thermal budget (TB) for dopants' diffusion, we discussed the influence of the pinhole density in the thermally grown SiO_x layer on the doping profiles and the passivation quality of double side textured n^+ and p^+ ion-implanted poly-Si passivating contacts. It is found that, for both n^+ and p^+ poly-Si samples, the existence of pinholes can enhance their passivation quality, if the pinhole density and the post-annealing TB are moderate ($\sim 1\times10^7$ cm^{-2} and $\sim 2\times10^{-12}$ cm^2, respectively). Also, we found that the sensitivity of passivation quality on the pinhole density for n^+ poly-Si samples is much higher than that for p^+ poly-Si samples. The enhanced passivation quality is due to the strengthening of the electrical field passivation, owning to the local diffusion of dopants through the pinholes.

CRediT authorship contribution statement

Guangtao Yang: Writing – original draft, Supervision, Data curation. **Remon Gram:** Data curation. **Paul Procel:** Formal analysis. **Can Han:** Formal analysis. **Zhirong Yao:** Formal analysis. **Manvika Singh:** Formal analysis. **Yifeng Zhao:** Formal analysis. **Luana Mazzarella:** Formal analysis. **Miro Zeman:** Formal analysis. **Olindo Isabella:** Supervision, Writing – review & editing.

Declaration of competing interest

The authors declare that they have no known competing financial interests or personal relationships that could have appeared to influence the work reported in this paper.

Data availability

Data will be made available on request.

References

[1] A. Richter, R. Müller, J. Benick, F. Feldmann, B. Steinhauser, C. Reichel, A. Fell, M. Bivour, M. Hermle, S.W. Glunz, Design rules for high-efficiency both-sides-contacted silicon solar cells with balanced charge carrier transport and recombination losses, Nat. Energy 6 (2021) 429–438.

[2] R. Peibst, C. Kruse, S. Schäfer, V. Mertens, S. Bordihn, T. Dullweber, F. Haase, C. Hollemann, B. Lim, B. Min, R. Niepelt, H. Schulte-Huxel, R. Brendel, For none, one, or two polarities—how do POLO junctions fit best into industrial Si solar cells? Prog. Photovoltaics Res. Appl. 28 (2020) 503–516.

[3] G. Nogay, J. Stuckelberger, P. Wyss, Q. Jeangros, C. Allebé, X. Niquille, F. Debrot, M. Despeisse, F.-J. Haug, P. Löper, C. Ballif, Silicon-rich silicon carbide hole-selective rear contacts for crystalline-silicon-based solar cells, ACS Appl. Mater. Interfaces 8 (2016) 35660–35667.

[4] B.L.J. Geerligs, M.K. Stodolny, Y. Wu, A. Gutjahr, G.J.M. Janssen, J. Anker, E. Bende, H. Ciftpinar, M. Lenes, J.-M. Luchies, LPCVD polysilicon passivating contact, Work. Cryst. Silicon Sol. Cells Modul. Mater. Process. (2016) 28–31.

[5] M. Rienäcker, A. Merkle, U. Römer, H. Kohlenberg, J. Krügener, R. Brendel, R. Peibst, Recombination Behavior of Photolithography-free Back Junction Back Contact Solar Cells with Carrier-Selective Polysilicon on Oxide Junctions for Both Polarities, Energy Procedia, 2016, pp. 412–418.

[6] G. Yang, A. Ingenito, N. Van Hameren, O. Isabella, M. Zeman, Design and application of ion-implanted polySi passivating contacts for interdigitated back contact c-Si solar cells, Appl. Phys. Lett. 108 (2016), 033903.

[7] Y. Chen, D. Chen, C. Liu, Z. Wang, Y. Zou, Y. He, Y. Wang, L. Yuan, J. Gong, W. Lin, X. Zhang, Y. Yang, H. Shen, Z. Feng, P.P. Altermatt, P.J. Verlinden, Mass production of industrial tunnel oxide passivated contacts (i-TOPCon) silicon solar cells with average efficiency over 23% and modules over 345 W, Prog. Photovoltaics Res. Appl. 27 (2019) 827–834.

[8] A. Ingenito, G. Limodio, P. Procel, G. Yang, H. Dijkslag, O. Isabella, M. Zeman, Silicon solar cell architecture with front selective and rear full area ion-implanted passivating contacts, Sol. RRL. 1 (2017), 1700040.

[9] W. Wu, J. Bao, L. Ma, C. Chen, R. Liu, Z. Qiao, J. Chen, Z. Liu, Development of industrial n-type bifacial TOPCon solar cells and modules, 36th Eur. Photovolt. Sol. Energy Conf. Exhib. Dev. (2019) 2–5.

[10] J. Krügener, F. Haase, M. Rienäcker, R. Brendel, H.J. Osten, R. Peibst, Improvement of the SRH bulk lifetime upon formation of n-type POLO junctions for 25% efficient Si solar cells, Sol. Energy Mater. Sol. Cells 173 (2017) 85–91.

[11] N. Nandakumar, J. Rodriguez, T. Kluge, T. Groβe, L. Fondop, P. Padhamnath, N. Balaji, M. König, S. Duttagupta, Approaching 23% with large-area monoPoly cells using screen-printed and fired rear passivating contacts fabricated by inline PECVD, Prog. Photovoltaics Res. Appl. 27 (2019) 107–112.

[12] M. Stodolny, K. Tool, B. Geerligs, J. Loffler, A. Weeber, Y. Wu, J. Anker, X. Lu, J. Liu, P. Bronsveld, A. Mewe, G. Janssen, G. Coletti, PolySi Based Passivating Contacts Enabling Industrial Silicon Solar Cell Efficiencies up to 24%, Prepr. 46th IEEE PV Conf, Chicago, 2019, pp. 1456–1459.

[13] R. Peibst, U. Römer, Y. Larionova, M. Rienacker, A. Merkle, N. Folchert, S. Reiter, M. Turcu, B. Min, J. Krugener, D. Tetzlaff, E. Bugiel, T. Wietler, R. Brendel, Working principle of carrier selective poly-Si/c-Si junctions: is tunnelling the whole story? Sol. Energy Mater. Sol. Cells 158 (2016) 60–67.

[14] H. Steinkemper, F. Feldmann, M. Bivour, M. Hermle, Numerical simulation of carrier-selective electron contacts featuring tunnel oxides, IEEE J. Photovoltaics 5 (2015) 1348–1356.

[15] P. Procel, G. Yang, O. Isabella, M. Zeman, Numerical simulations of IBC solar cells based on poly-Si carrier-selective passivating contacts, IEEE J. Photovoltaics 9 (2019) 374–384, https://doi.org/10.1109/JPHOTOV.2019.2892527.

[16] R. Regner, An analytical approach to quantify the thermal budget in consideration of consecutive thermal process steps, in: 10th IEEE Int. Conf. Adv. Therm. Process. Semicond., IEEE, 2002.

[17] F. Feldmann, J. Schön, J. Niess, W. Lerch, M. Hermle, Studying dopant diffusion from Poly-Si passivating contacts, Sol. Energy Mater. Sol. Cells 200 (2019), 109978.

[18] Z. Yang, J. Krügener, F. Feldmann, J.I. Polzin, B. Steinhauser, T.T. Le, D. Macdonald, A.Y. Liu, Impurity gettering in polycrystalline-silicon based passivating contacts - the role of oxide stoichiometry and pinholes, Adv. Energy Mater. (2022) 1–11, 2103773.

[19] J.Y. Gan, R.M. Swanson, Polysilicon emitters for silicon concentrator solar cells, in: Proceedings of IEEE 21st Photovoltaic Specialists Conference, PVSC), 1990, pp. 245–250.

[20] U. Römer, R. Peibst, T. Ohrdes, B. Lim, J. Krügener, E. Bugiel, R. Brendel, Recombination behavior and contact resistance of n+ and p+ poly-crystalline Si/mono-crystalline Si junctions, Sol. Energy Mater. Sol. Cell. 131 (2014) 85–91.

[21] R.A. Sinton, A. Cuevas, Contactless determination of current-voltage characteristics and minority-carrier lifetimes in semiconductors from quasi-steady-state photoconductance data, Appl. Phys. Lett. 69 (1996) 2510–2512.

[22] T.F. Wietler, D. Tetzlaff, J. Krügener, M. Rienäcker, F. Haase, Y. Larionova, R. Brendel, R. Peibst, Pinhole density and contact resistivity of carrier selective junctions with polycrystalline silicon on oxide, Appl. Phys. Lett. 110 (2017).

[23] T.N. Truong, D. Yan, W. Chen, W. Wang, H. Guthrey, M. Al-Jassim, A. Cuevas, D. Macdonald, H.T. Nguyen, Deposition pressure dependent structural and optoelectronic properties of ex-situ boron-doped poly-Si/SiOx passivating contacts based on sputtered silicon, Sol. Energy Mater. Sol. Cells 215 (2020).

[24] A. Fell, F. Feldmann, C. Messmer, M. Bivour, M.C. Schubert, S.W. Glunz, Adaption of basic metal – insulator – semiconductor (MIS) theory for passivating contacts within numerical solar cell, Modeling 8 (2018) 1546–1552.

[25] J.S. Christenser, H.H. Radamson, A.Y. Kuznetsov, B.G. Svensson, Phosphorus and boron diffusion in silicon under equilibrium conditions, Appl. Phys. Lett. 82 (2003) 2254–2256.

[26] K. Shimakura, T. Suzuki, Y. Yadoiwa, Boron and phosphorus diffusion through an SiO2 layer from a doped polycrystalline Si source under various drive-in ambients, Solid State Electron. 18 (1975) 991.

[27] A. Kale, S.U. Nanayakkara, W. Nemeth, H. Guthrey, M. Page, M. Al-Jassim, S. Agarwal, Scanning kelvin probe microscopy: a tool to investigate nano-scale doping non-uniformities in poly-Si/SiOx contacts, Preprint. Golden, CO: National Renewable Energy Laboratory. NREL/CP-5900-73161, https://www.nrel.gov/docs/fy20osti/73161.pdf.

[28] M. Fırat, L. Wouters, P. Lagrain, F. Haase, J. Polzin, A. Chaudhary, J. Poortmans, Local enhancement of dopant diffusion from polycrystalline silicon passivating contacts, ACS Appl. Mater. Interfaces 14 (15) (2022) 17975–17986.

[29] F. Feldmann, G. Nogay, J.I. Polzin, B. Steinhauser, A. Richter, A. Fell, S.W. Glunz, A study on the charge carrier transport of passivating contacts, IEEE J. Photovoltaics 8 (6) (2018) 1503–1509.

[30] F. Feldmann, J. Schoen, J. Niess, W. Lerch, M. Hermle, Studying dopant diffusion from poly-Si passivating contacts, Sol. Energy Mater. Sol. Cell. 200 (2019), 109978.